

Contents lists available at ScienceDirect

# Composites Part B

journal homepage: www.elsevier.com/locate/compositesb



# Check for updates

# Hybrid green composites using rice straw and jute fabric as reinforcement for soy protein-based resin

Abdullah Alkandary a,b, Anil N. Netravali c,\*

- <sup>a</sup> Materials Science and Engineering, Cornell University, Ithaca, NY, USA
- <sup>b</sup> Nanotechnology and Advanced Materials Program, Kuwait Institute for Scientific Research, Kuwait City, Kuwait
- <sup>c</sup> Human Centered Design, Cornell University, Ithaca, NY, USA

#### ARTICLE INFO

Handling Editor: Dr Uday Vaidya

#### Keywords:

- A. Hybrid green composites
- A. Hybrid
- B. Mechanical properties
- B. Fiber/matrix bond

#### ABSTRACT

In this research, high amounts of the world's most wasted agricultural residue (rice straws) were utilized to produce hybrid green composites. Rice straws (RS) were needle-punched into jute fabric to form hybrid reinforcement mats which were impregnated with a soy protein isolate resin (SPR). Thermoset hybrid composites were produced at three different fiber contents of 40, 50, and 60% by wt. They were characterized for their tensile, flexural, interfacial, fractural, and hygroscopic properties. The hybrid composites with 40% fiber content enhanced Young's modulus  $(E_v)$  and ultimate tensile strength (TS) of the pure resin by 200% and 47%, respectively, compared to pure resin. With increasing fiber content, mechanical properties such as  $E_v$ , TS, flexural modulus, and flexural strength decreased, indicating insufficient resin volume. Interfacial shear strength values of RS/SPR and Jute/SPR were measured at 2.68 and 4.25 MPa, respectively. The high volumes of low-density RS and higher viscosity of the resin used in the hybrid composites seemed to overwhelm the resin's capacity to effectively wet the fibers. Insufficient wetting and low interfacial shear strength (IFSS) resulted in fiber pull-outs at fracture surfaces. Furthermore, as fiber content increased from 40 to 50 to 60%, moisture absorption increased from 10.4 to 12.9 to 22.6%, respectively. This is in spite of the fact that SPR was the most hydrophilic component of the three constituents. These results suggest that the high volumes of low-density fibers induce structural defects and exhaust the resin's wettability. Overall, the hybrid biodegradable composites had good tensile properties for use in packaging, transportation, housing, and furniture.

# 1. Introduction

The term 'green composites' emerged during the late 20th century to describe compostable and fully sustainable polymer matrix composites (PMCs) of plant origins, that strictly contain no petroleum-based polymers or chemicals [1–3]. Green composites have a significant advantage of not needing to separate the constituents for their end-of-life processing, as they can be easily disposed of or composted. In fact, when composted, they create soil-enriching organic fertilizer. As a result, they can be expected to solve major issues that accompany the production and disposal of conventional petroleum-based PMCs. Since conventional petroleum-based polymers can take several centuries to degrade, conventional composites overload the landfills for long periods of time without biodegrading [4]. It is estimated that by the year 2050 and at the current production rate, 12,000 million metric tons (Mt) of plastic waste, including composites, would occupy landfills around the world,

taking away much needed space for the natural environment [5]. Furthermore, the production process of polymers and composites would contribute to 15% of the global carbon budget by that time [6]. Petroleum-based materials currently dominate the PMC market [1]. This can be attributed to the significant investment in these materials by governments and industries to conduct research, manufacture, and reduce their cost following the boom of the petrochemical industry post-World War II [7]. Consequently, conventional PMCs became integral to numerous applications, even those where their high specific (or 'advanced') properties and bio-resistivity were not needed, such as low-mechanical stress resisting structures.

Soy protein isolate (SPI) is a coproduct of the soybean process that contains more than 90% protein by weight. Soy protein is the most produced edible plant protein [8], and the research on its adhesive properties dates back to the 1920s [9]. Since then, soy-based adhesives were commercialized in the plywood and automotive industries, right

E-mail address: ann2@cornell.edu (A.N. Netravali).

<sup>\*</sup> Corresponding author.

until the synthetic formaldehyde-based adhesives emerged in the 1960s [9-11]. Soy protein consists of 19-20 different amino acids, with glycinin 7S and  $\beta$ -conglycinin 11S (where S denotes a Svedberg unit [12]). These two proteins make up about 87% of soy's protein content [13–15]. The abundance of functional groups on soy protein, i.e., peptide chains (e.g., amino, hydroxyl, carboxyl, and sulfhydryl groups), enables both self- or external-crosslinking [16]. To prepare crosslinked SPI, the protein must be denatured from its isoelectric point of about 4.5 pH, to avoid SPI neutral charge which results in chain entanglement (globular) and, hence, coagulation and poor water-solubility [16]. Moreover, denaturing exposes the functional groups in SPI, thus availing them to chemical reactions. Many chemical compounds have been reported to crosslink SPI including sugar-aldehydes, glyoxal, and glutaraldehyde [12,17-28]. Glutaraldehyde (GA) has a boiling point of 187 °C and exhibits a high reactivity at room temperature with  $\varepsilon$ -amino, amino acid residue, and other nucleophilic groups present in SPI [11,27]. GA crosslinks SPI through the Maillard reaction shown in Fig. 1 [11,28].

Plant fibers are natural composite materials composed of amorphous hemicellulose, lignin, and pectins that are reinforced by fibrillar crystalline cellulose. Jute (*Corchorus capsularis*) fibers produced from the plant stem have Young's modulus ( $E_y$ ), tensile strength (TS), and density values within the ranges of 10–60 GPa, 393–860 MPa, and 1,300–1,520 kg/m³, respectively [29–31]. Jute fibers are produced in plentiful and are conventionally spun into yarns to be used in packaging, textiles, footwear, and ropes [32]. Also, their use in automotive paneling has been rising since the 1990s [30].

Another natural fiber which has recently gained wide interest in reinforcing PMCs is rice straw-the structural part of the rice plant (Oryza sativa L.) [33-37]. The rice industry produces the world's largest crop residue, with approximately 800 Mt of dry biomass annually because of the high demand for rice [38,39]. The disposal of rice straw has been challenged by its silica content, which makes it a harsh material with low digestibility and a less favored fodder for cattle [38]. Hence, many rice farmers have resorted to the hazardous open field burning of rice straw. It is the quickest and least expensive method to dispose dry residue, control weeds and diseases, and release nutrients into the soil [39]. However, this irresponsible practice releases high amounts of toxic greenhouse gases and aerosolized black carbon into the environment. It has been reported that Thailand, Egypt, China, India, and the Philippines burn alarming proportions of rice straw residue, reaching 48% (2002–2006), 53% (2013), 62% (1995–2005), 62% (1999–2000 and 2004-2005), and 95% (2002-2006), respectively [40]. Rice straw itself is a low-density natural fiber, with baled and pelleted rice straw densities ranging between 60 and 450 kg/m<sup>3</sup> and 560-800 kg/m<sup>3</sup>, respectively [41-45].

The present research focuses on preparing green composites that include high masses of rice straw, following an accessible and facile manufacturing process [46]. A layer of rice straw fibers and jute fabric was mechanically felted (needle-punched) together into a condensed reinforcement mat. These mats were impregnated with the SPI-based resin, stacked in triple layers and cured in a hot press machine to form composites. The resulting hybrid composites were characterized for their mechanical, fractural, and moisture sorption characteristics. Furthermore, the constituent materials were separately characterized

for the same properties. In addition, the interfacial shear strength between each fiber type and the SPI-based resin was studied through a microbond test. Results of the study suggest that these hybrid green composites would be suitable for use in sustainable furniture, housing, transportation, and packaging applications replacing currently used wood and wood-based products.

#### 2. Material and methods

#### 2.1. Materials

SPI was donated by the Archer-Daniels-Midland Company (Chicago, IL). Glutaraldehyde (GA) solution (25%) in  $\rm H_2O$  was purchased from Sigma-Aldrich (St. Louis, MO) and high-purity D-sorbitol was purchased from VWR International, LLC (Solon, OH). Sodium hydroxide (NaOH) pellets were purchased from Avantor Performance Materials, LLC (Radnor, PA). Untreated plain-woven jute fabric was purchased from JOANN Fabrics and Crafts (Ithaca, NY). Baled rice straw was purchased from Engine 109 The Bulk Depot (Hollister, CA).

#### 2.2. Preparation of SPI resin (SPR)

SPI powder was dispersed in deionized water (at a 3:20 SPI:water ratio) and continually stirred at 600 rpm using a magnetic stirrer to form a homogenous protein slurry. Alkali denaturing of the protein was achieved by adding 4 M NaOH solution to the slurry until a  $12.5\pm0.1$  pH level was achieved. The alkali SPI slurry was placed in an  $80^{\circ}\text{C-water}$  bath for 30 min under same stirring conditions. After that, plasticizer (D-sorbitol) at 5 wt% of SPI and GA at 10 wt% of SPI were added and stirred for another 30 min for partial curing.

The partially cured (also known as B-stage) resin was poured into Teflon molds and evaporated in an open-vent convection oven (Thermo Fisher Scientific Co., Model No. PR305225 M, Waltham, MA) at 46 °C to reach a moisture content of  $\sim\!12\%$ . The semidry resin sheets were cured in a hot press machine (Carver Inc., model 3981-4PROA00, Wabash, IN) under 140 °C and 1 MPa pressure for 5 min to fully set. The resin sheets had thicknesses of around 1.5 mm, and were laser cut to dimensions compatible with the corresponding tests.

#### 2.3. Preparation of hybrid composites

A schematic illustration of the preparation process is illustrated in Fig. 2. Rice straws (RS) were washed twice with tap water and left to dry for 3 h under 50 °C in the convection oven. Untreated woven jute fabric (JFa) was used as-received. It was cut to  $0.254~\text{m}\times0.254~\text{m}$  square mats and weighed on a digital microscale. Each JFa mat mass was matched with that of dry RS, to maintain a 1:1 mass ratio between the two. The RS were randomly spread on top of the square JFa and softened with ~10 ml deionized water. Then the fibers were mechanically needle-punched to form a hybrid mat by passing them through an automated needle-punching machine (FeltLOOM® PRO SERIES, Sharpsburg, KY) ten times at 20% roller speed and 50% needle speed. Needle-punching (or felting) is a common technique used in the textile and non-woven industry, which employs barbed needles to interlace fibers to produce

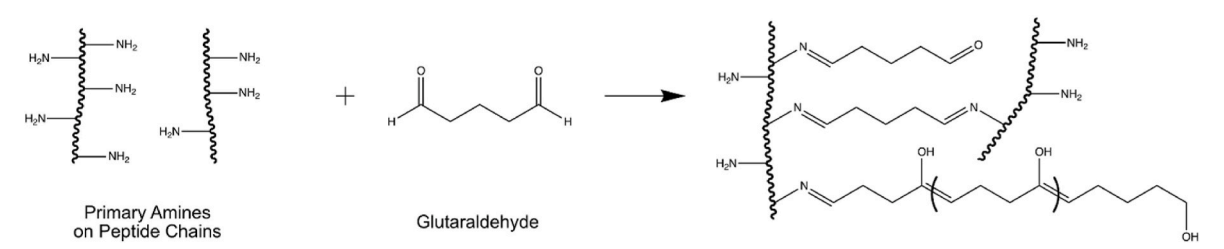
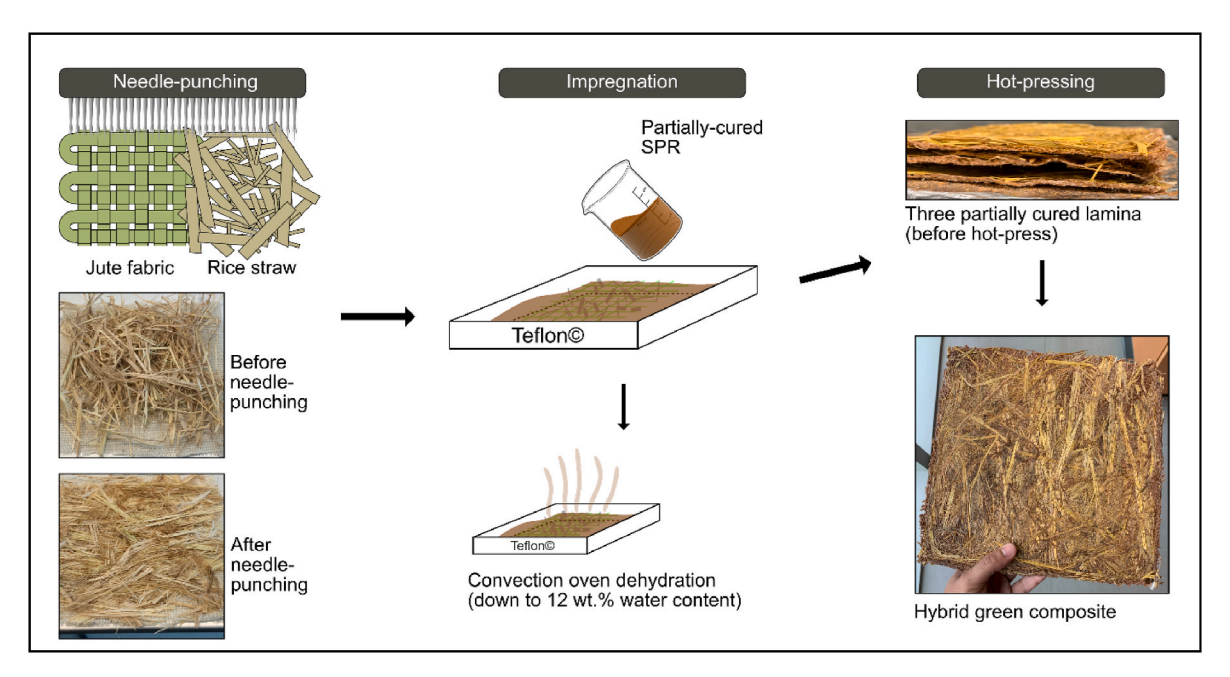


Fig. 1. Primary amine and glutaraldehyde (Maillard) crosslinking mechanism.



**Fig. 2.** Schematic illustration of hybrid composite fabrication process, starting with needle-punching of RS and JFa, followed by partially-cured SPR impregnation of reinforcement, then curing layered lamina using a hot-press method.

'needle-punched' mats. Images of the fibers before and after needle-punching are presented in Fig. 2. The hybrid mats were then individually placed in Teflon® molds and completely dried before being massaged thoroughly with the B-staged resin. The resin-soaked mats were dried down to  $\sim\!12\%$  water content in the oven under 46 °C for around 45 h. Following that, the semidry resin-impregnated mats were stacked in layers of three (with JFa's warp/weft directions preserved) before hot-pressing at 140 °C under a pressure of 4.1 MPa for 5 min to fully cure (using a Carver Inc., Model No. 3895.4NE0000, Wabash, IN). Three fiber (JFa + RS) contents (namely, 40%, 50%, and 60%) by mass were used to fabricate three composite systems. Following nomenclature was used to identify the three composites: HC40, HC50, and HC60; where 'HC' refers to 'hybrid composite' and the numbers correspond to % fiber content.

### 2.4. Water absorption

All specimens (i.e., fibers, resins, and their composites) were characterized for mass gains due to moisture absorption under the conditions of 21  $^{\circ}\text{C}$  and a RH of 65% for 72 h. The composites were also examined for their dimensional changes (width and thickness gains) induced by moisture absorption.

# 2.5. Tensile properties of fibers

Cylinder-like RSs were carefully slit along their longitudinal axis and opened up into rectangular sheets. This way, the surface area measurements could be more accurate by eliminating the fiber lumen (core space). The specimens were glued with cyanoacrylate glue (Krazy Glue<sup>®</sup>) on paper tabs that had a 25 mm gap between the two glued spots, representing the gauge length, and in compliance with ASTM D3822/D3822 M - 14 (2020) recommendations for natural fibers. Specimen width was measured using a digital caliper (Fowler High Precision, Model No. Pro-Max PN 54-200-777, Auburndale, MA) and the thickness was measured using an optical microscope (Olympus Corp., Model No. BX51, Hamburg, Germany) using a 10× objective lens after each tensile test. The tensile tests were performed on an Instron universal testing machine (Instron, Instron Corp., Model No. 5566, Canton, MA) with a 10 kN load cell. Paper tabs holding RS were clamped with a 25 mm

gauge length and a strain rate of  $0.004\,\mathrm{min}^{-1}$  were used to achieve break between 1 and 2 min. While ASTM D3822/D3822 M - 14 (2020) does not specify a time limit on the test, the experiment was set at a conservative 1 to 2 min time frame. Moderate pretest conditions (varied from 1 MPa to 5 MPa based on specimen) were used to straighten up the fibers prior to testing.

Plain-woven JFa was tensile tested according to the fabric strip test ASTM 5035-11 (2019) as shown in Fig. 3. The tests were carried along both directions of the weave, i.e., longitudinal 'warp' and transverse 'weft' directions. According to textile nomenclature, the warp yarns are those that were aligned (under cyclic tension) and placed along the length of the fabric during weaving, in order for the weft yarns to be woven perpendicularly, according to desired pattern. Hence, the warp direction is generally known to exhibit higher strength and stiffness than the weft. The fabric thickness was measured using a compressometer (Frazier Precision Instrument Company Inc., Hagerstown, MD) and a 9.525 cm diameter presser foot. Five measurements were taken for each specimen at a pressure of 17.2  $\pm$  4.9 kPa. All JFa specimens were cut to a 30 mm width and axial varns were unraveled to a 25 mm width (as seen in Fig. 3a and b) with a consistent number of axial varns (i.e., seven varns), as per ASTM 5035-11 (2019). Moreover, a gauge length of 30 mm and strain rate of 0.167 min<sup>-1</sup> were used to achieve the ASTM 5035-11 (2019) recommended break time, between 0.5 and 5 min.

Jute yarns (JY) were unraveled from JFa and tensile tested according to ASTM 2256–10. A gauge length of 30 mm was used. The strain rate to achieve a break at around 20 s was determined to be 0.133  $\rm min^{-1}$ . A pretest tension of 2 MPa was applied to eliminate yarn crimp. The thickness of JY was measured using the same method as JFa, and it was taken as the diameter of the outer *cylindrical sleeve* of the yarn geometry.

Prior to tensile testing, all fibers and fabrics were conditioned at 21  $^{\circ}$ C and 65% RH for 48 h as per ASTM D1776–04.

#### 2.6. Tensile properties of SPR

Resin sheets were laser-cut to  $70\times5$  mm strips to maintain a 6:1 ratio between gauge length (which was 30 mm) and width. Specimens were conditioned at ASTM conditions of 21 °C and 65% RH for 72 h prior to testing. SPR specimens were directly clamped onto the Instron and tested according to ASTM D638–14 using a crosshead speed of 5

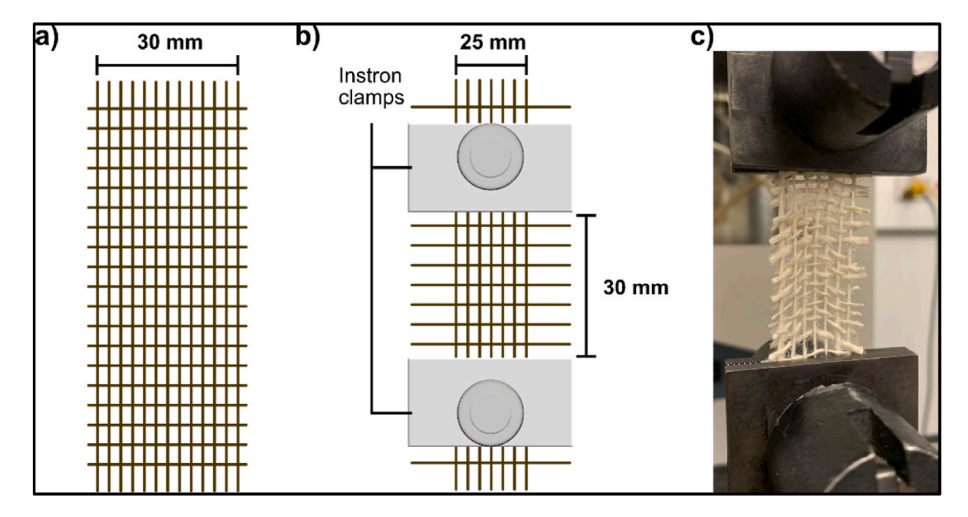


Fig. 3. Jute fabric tensile setup according to fabric strip test ASTM 5035–11 (2019); where a) fabric specimen of 30 mm width, b) unraveled specimen directly clamped to Instron, and c) actual specimen under test.

mm/min (strain rate of  $0.167~\text{min}^{-1}$ ) to cause ductile rupture between 0.5~and~5~min.

#### 2.7. Fiber/resin interfacial shear strength (IFSS)

The fiber/SPR interfacial shear strength (*IFSS*) values were obtained through the microbond test which is a modification of the conventional fiber-pullout test [12]. The experimental procedure for microbond test was similar to that used by previous researchers [3,12,20,47–50]. A hydrophobic ultrahigh molecular weight polyethylene (UHMWPE) fiber was dipped into B-staged (partially cured) SPR and taken out to obtain a droplet of SPR at the tip of the fiber. The droplet was put in contact with the hydrophilic fiber, RS or JF, being held horizontally, allowing differential surface energies to naturally transfer the droplet from UHMWPE fiber onto RS or JF. The SPR droplets on individual fibers were cured in the forced-air convection oven at 110 °C for 30 min. The cured specimens were conditioned at 21 °C and 65% RH for 72 h to equilibrate their water content prior to testing.

The fiber/resin contact length and fiber diameter in JF/SPR specimens were measured using the Olympus microscope mentioned earlier and ImageJ image processor whereas the RS/SPR dimensions of interest (i.e., fiber/resin contact length, and fiber width and thickness) were measured using the digital caliper. The experimental setup is shown in Fig. 4, where the paper tab was clamped to the Instron machine and two micro-vice blades were held fixed to prevent the resin droplet from crossing them as the paper tab is being vertically pulled; by that inducing shear forces at the fiber/resin interface. *IFSS* tests were carried out on an Instron with a 100 N load cell and 0.2 mm/min crosshead speed, under 21 °C and 65% RH.

The maximum force ( $F_{max}$ ) recorded was assumed to be the force required to fully debond the microbead from the fiber; and the maximum interfacial shear strength ( $\tau_{max}$ ) was calculated according to Eq. (1) [3,20,51].

$$\tau_{max} = \frac{F_{max}}{A} \tag{1}$$

where *A* is the fiber/resin contact area.

# 2.8. Tensile and flexural properties of hybrid composites (HCs)

Each HC was tested under tension along both warp and weft directions (of jute fabric) after being conditioned according to ASTM D618–21 under 21  $^{\circ}$ C and 65% RH for 72 h. Given that RH employed was 15% higher than the ASTM recommendation of 50% for composites,

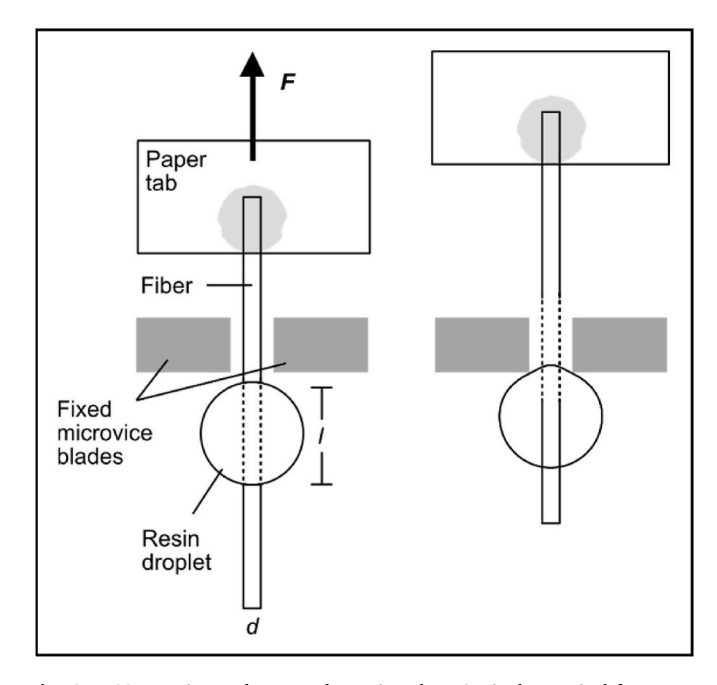


**Fig. 4.** IFSS experimental setup schematic; where 'F' is the vertical force vector, 'l' is the fiber/resin contact length, and 'd' is the fiber diameter.

it should be noted that the values of the mechanical properties of composites are conservative. The specimens were laser-cut to 110 mm  $\times$  10 mm rectangles. The gauge length and strain rate were 30 mm and 0.033  $\rm min^{-1}$ , respectively, to achieve failure between 0.5 and 5 min.

As for flexural properties, a three-point bend fixture was set up on the same Instron with the span length adjusted for each specimen to maintain a span-to-depth ratio between 16:1 and 20:1. The specimens were laser-cut to 120 mm  $\times$  12 mm rectangles and conditioned at 21 °C and 65% RH for 72 h before being tested according to ASTM D790–03. The testing rate was increased to 10 mm/min (as compared to ASTM recommendations) to observe rupture in the outer surface of the specimen before the 5% deflection mark. All JFa/RS-layered specimens were placed with the RS (weaker) side facing the bottom and the JFa side facing the top. The maximum flexural strength (*FS*) was found using Eq. (2) and the flexural modulus (*E<sub>f</sub>*) using Eq. (3) [52,53].

$$FS = \frac{3PL}{2wD^2} \tag{2}$$

where P is the peak load in MPa, L is the support span length in m, w is the specimen width in m, and D is the thickness of the specimen in m; and

$$E_f = \frac{L^3 m}{4wD^3} \tag{3}$$

where m is the slope of the initial linear portion of the stress-deflection curve in N/m.

#### 2.9. Rule of hybrid mixtures (ROHM)

The experimental results obtained from standard ASTM constituent tensile tests were incorporated into the widely used rule of hybrid mixtures (ROHM) [54–56], a modified version of the simple rule of mixtures (ROM). The ROHM deals with the hybrid reinforcements as multiple separate non-hybrid composites. A direct consequence of this assumption is neglecting the interaction between the separated composite systems which is unrealistic, particularly for the interlaced fiber reinforcements used in this study. Fig. 5 depicts a schematic of ROHM setup for hybrid composites (HC) and their corresponding axes. It is important to mention that, in addition to the previous assumptions, such a fixture assumes that laminae exhibit the same Poisson effects and null force interactions in between, and that all fibers are assumed to be axially aligned with the load axis.

Under isostress, the general volumetric mixture Eq. (4) and the subsequent sum of volume ratios Eq. (5) were used to find Young's modulus of the hybrid RS/JFa/SPR composite ( $E_{HC}$ ) according to ROHM [56].

$$E_{HC} = E_{C1}V_{C1} + E_{C2}V_{C2} \tag{4}$$

$$V_{C2} = 1 - V_{C1} \tag{5}$$

where  $E_{C1}$  and  $V_{C1}$  are Young's modulus and volume fraction of non-hybrid RS/SPR composite system, respectively, and  $E_{C2}$  and  $V_{C2}$  are Young's modulus and volume fraction of nonhybrid JFa/SPR composite system, respectively. The values of  $E_{C1}$  and  $E_{C2}$  are found using the simple rule of mixture (ROM) Eqs. (6) and (7) [29]:

$$E_{C1} = E_{f1}V_{f1} + E_mV_{m1} (6)$$

$$E_{C2} = E_{f2}V_{f2} + E_mV_{m2} \tag{7}$$

where E and V are the Young's moduli and the volume fractions, and

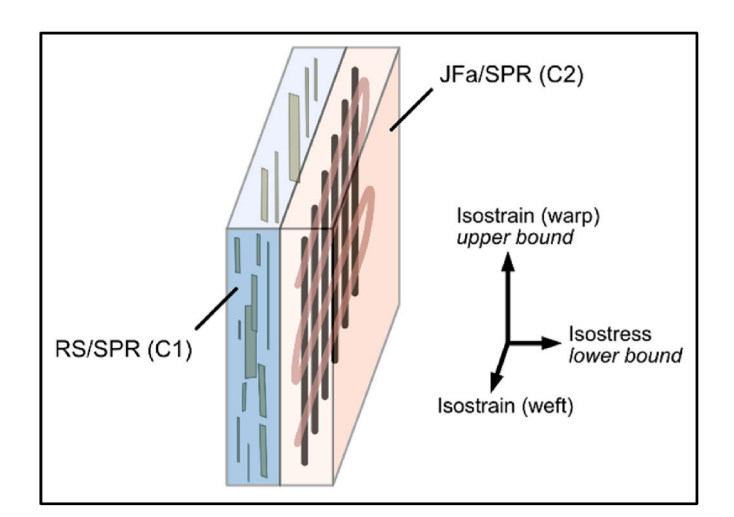


**Fig. 5.** Schematic of the separated RS/SPR and JFa/SPR composites according to ROHM. Note: illustration shown is of Isostrain-warp setup where RS is aligned in the warp direction.

subscripts f1, f2, m, m1, and m2 denote RS, JFa, resin (matrix), resin of RS/SPR composite, and resin of JFa/SPR composite, respectively. Using Eqs. (6) and (7), Eq. (4) can be rewritten as Eq. (8):

$$E_{HC} = (E_{f1}V_{f1} + E_mV_{m1})V_{C1} + (E_{f2}V_{f2} + E_mV_{m2})V_{C2}$$
(8)

Equation (8) calculates Young's modulus for the isostrain case—the upper bound of modulus.

Table 1 presents the volume fractions needed to solve for Eq. (8). These parameters were found through a mass-to-volume conversion using fiber densities, i.e., RS and JF, found in the literature to be approximately  $0.80 \text{ g/cm}^{31}$  and  $1.41 \text{ g/cm}^{3}$  [29–31,41–45], respectively.

#### 3. Results and discussion

#### 3.1. Water absorption

Mass and dimension gains by the hybrid composites due to water absorption were measured by conditioning the laser-cut specimens at 21 °C and 65% RH for 72 h. In addition, mass gains of composite constituents (i.e., JFa, RS, and SPR) were measured separately, under the same conditions. Fig. 6 visualizes the mass and dimension measurements after 72 h of conditioning.

The results show that RS gained a slightly higher mass percentage than JFa after conditioning (5.5% and 4.1%, respectively) which can be attributed to latter's higher crystalline cellulose content. SPR showed a mass gain of around 9.5%, which is 72% and 132% higher than those of RS and JFa, respectively. It is clear that the hydrophilic SPR is the dominant water absorbing component. This is also why the SPR gets plasticized after conditioning.

Composite specimens were laser-cut to identical lengths and widths, with mean thicknesses ranging between 3.10 and 3.58 mm. Thus, the surface area of the specimens was quite similar. Consequently, the composites gained statistically similar mass (moisture) percentages, ranging between 9.9 and 11.8% upon conditioning. Composite width gain was negligible, ranging between 0.6% and 1.1%. This was primarily because the fibers were placed with their longitudinal dimension perpendicular to the composite thickness. Fibers do not change their length much when they absorb moisture. As seen earlier, fibers do not absorb as much moisture as the SPR. As a result, swelling in the transverse direction (the width) was minimal. While gains in thicknesses were found to increase with fiber content: 10.4, 12.9, and 22.6% for HC40, HC50, and HC60, respectively. This is an indication of the resins being overloaded with fibers at higher fiber content.

#### 3.2. Fiber/resin IFSS characterization

Fig. 7a illustrates typical force-displacement curves of the microbond tests performed on RS/SPR and JF/SPR specimens. The mean *IFSS* values were  $4.25 \pm 1.78$  MPa and  $2.68 \pm 1.30$  MPa for JF and RS fibers, respectively, with a distinguishable statistical confidence (P=0.012,  $\alpha$ 

Table 1
Volume fractions needed to solve ROHM for HC, C1, and C2 composite systems.

Composite	$V_{C1}$	$V_{m1}$	$V_{m2}$	$V_{f1}$	$V_{f2}$
HC40	0.54	0.67	0.79	0.33	0.21
HC50	0.55	0.58	0.71	0.42	0.29
HC60	0.56	0.48	0.62	0.52	0.38

 $<sup>^{1}</sup>$  The RS density value is the average between bale and pelleted RS densities found in the cited works, since RS in this study was received as bale, felted, and then hot-pressed.

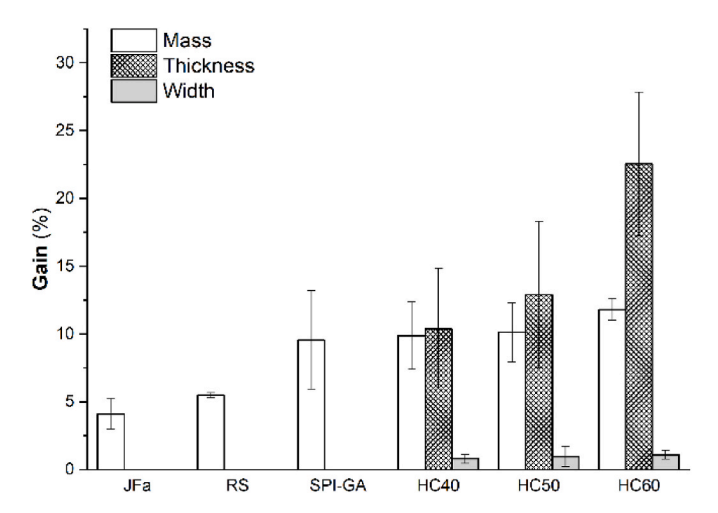


Fig. 6. Mass and/or dimension percent gains due to water absorption for JFa, RS, SPR, and their composites.

= 0.05). JF/SPR debonding character resembled that of typical shear debonding, as seen in the spike shown in Fig. 7a which indicates the specimen's consensus shear load resistance. RS/SPR interface on the other hand, resists the load up until nearly half its IFSS value after which droplet slippage occurs, as established by Miller et al. [57], seen as an extended low-slope line in the force-displacement curve in Fig. 7a. The IFSS results were examined for their correlation to fiber/microbead contact area, and the results are found in Fig. 7b. With exception to JF's two outliers at realatively low contact area. IFSS values of all specimens fluctuated around their means with respect to their normalized contact area. The reason behind the difference in IFSS values between JF or RS and SPR is the higher surface roughness of JFs, as well as their overall structure consisting of a bundle of short fibers that provide more interspatial surface area (as seen in Fig. 8a and b). As a result, JF is expected to exhibit a better fiber/resin interface, primarily due to enhanced mechanical interlocking [58,59]. The hydrophilicity of the resin is evident from the low contact angle of the microbead's edges around the JF seen in Fig. 8c, where a fully cured SPR bead completely surrounds a JF, before microbond test. Furthermore, after the pull-out test, complete debonding was observed from the spatial gaps between the bead and the fiber as seen in Fig. 8d.

## 3.3. Tensile properties

Ideal response of composites to tensile load can be predicted according to the rule of hybrid mixtures (ROHM), which requires constituents' individual TS and  $E_y$  as inputs, in addition to their volumetric ratios in the composites. The tensile properties of RS, JFa, JY, SPR, and

their composites at different fiber contents are illustrated in Fig. 9 and are discussed in the following subsections.

#### 3.3.1. Constituent tensile properties

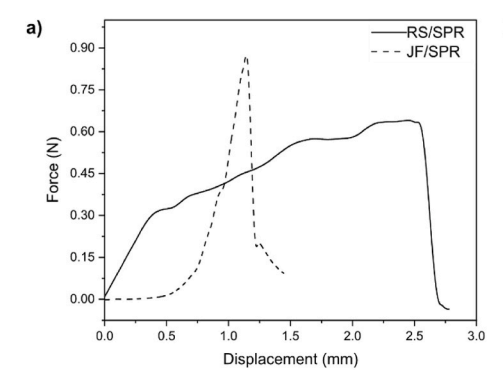
Fig. 9a presents selected tensile properties of the constituents: SPR, JFa, JY, and RS. Preliminary experiments were performed to prepare SPR with a strain at *TS* of at least double that of the more brittle fiber in the hybrid system—i.e., RS. Results obtained confirm that the strain criterion was satisfied with SPR-to-RS strain at *TS* exceeding 5.5-to-1.

The tensile properties of fibrous assemblies and their composites depend primarily on the fiber properties and the geometry of the assembly. Staple fibers, such as JF used in this work, are often twisted into yarns to induce inter-fiber friction and cohesiveness through which strength of the yarn is realized. However, twisting has its implications on the assembly's mechanics. Particularly, stiffness is reduced as fibers twist into yarns [60,61]. Weaving yarns into fabric introduces even more loss in stiffness and strength due to crimp, thread spacing, and thread density [62]. A notable decline in TS can be seen when comparing JY to JFa, which can be attributed to the actual packing factor of JY being lower than the idealized varn sleeve measurement. Furthermore, given that diameter and thickness measurements for JY and JFa, respectively, were identical; it is important to note that ASTM 5035-11 fabric test standard does not factor out the space between the yarns in the fabric. As a result, the area under stress in the case of JFa is highly exaggerated, and therefore, the strength shows a much lower value. JFa in warp direction (20 MPa) is evidently stiffer and stronger than the weft direction (14.8 MPa) as seen in Fig. 9b. Warp threads are intentionally made stronger so they can survive the cyclic stresses experienced during weaving. Like all natural fibers, RSs exhibit a broad range in physical and mechanical properties. The mean  $E_v$  and TS values of the tested RS were 2.2  $\pm$  1.7 GPa and 31.4  $\pm$  25.2 MPa, respectively.

In addition to the well documented factors causing natural fiber property variability (i.e., rice variety, geographic region, weather, season, harvesting methods, plant age, etc. [63]), the architecture of RS also adds to the variability. RS have sites of thicker epidermis tissue, similar to bamboo and known as nodes, that reinforce the vertical growth of the plant. The internodal regions (region between two nodes) are weaker and more compliant.

#### 3.3.2. Composite theoretical tensile properties

The differences between the theoretical (ROHM) and experimental results presented in Fig. 9b are quite clear. For instance, experimental  $E_y$  results in warp direction were between 24.7% and 63.7% lower than predicted and similar deviation was found for TS in the warp to be between 45.8% and 65.0%. A major contributor to this gap was the water absorption capacities of the hydrophilic constituents (discussed in Section 3.1) which is not accounted for in ROHM. Additionally, theoretical ROHM calculations assume ideal fiber axial orientation, null force interactions between laminae, as well as fiber continuity. None of these



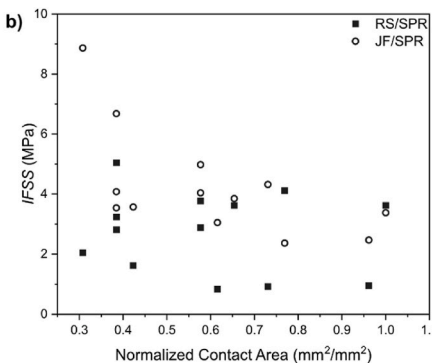


Fig. 7. IFSS microbond test results for RS/SPR and JF/SPR, where a) typical force-displacement curves, and b) IFSS data points as a function of normalized contact area. N = 13 for JF and N = 20 for RS.

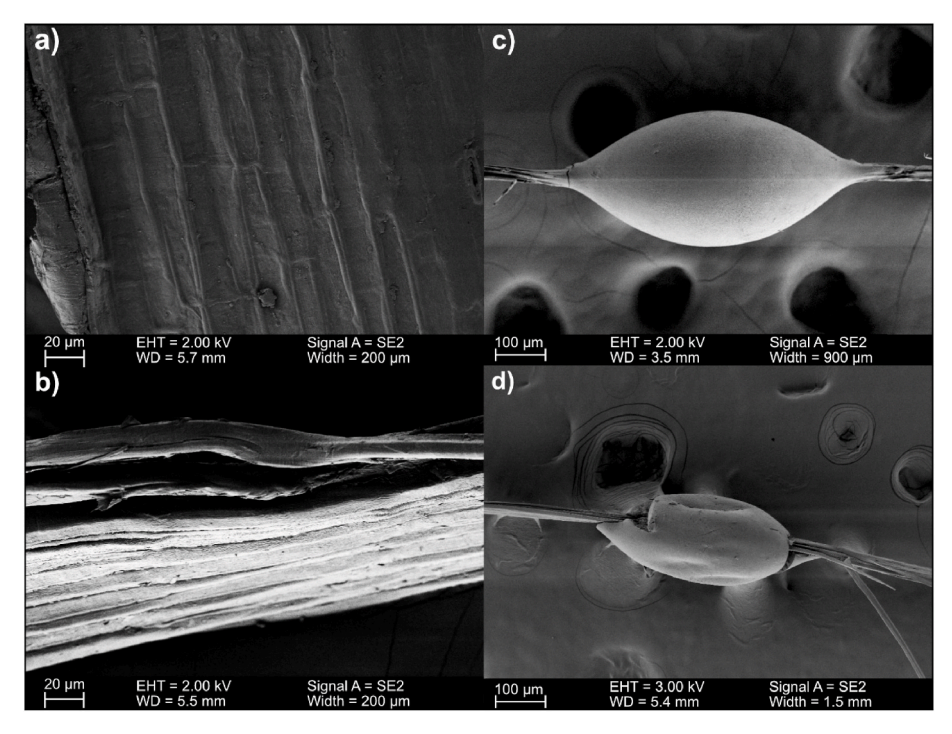


Fig. 8. SEM images of a) rice straw fiber surface, b) jute fiber surface, c) SPR microbead on jute fiber before microbond test, and c) SPR microbead and jute fiber after microbond test.

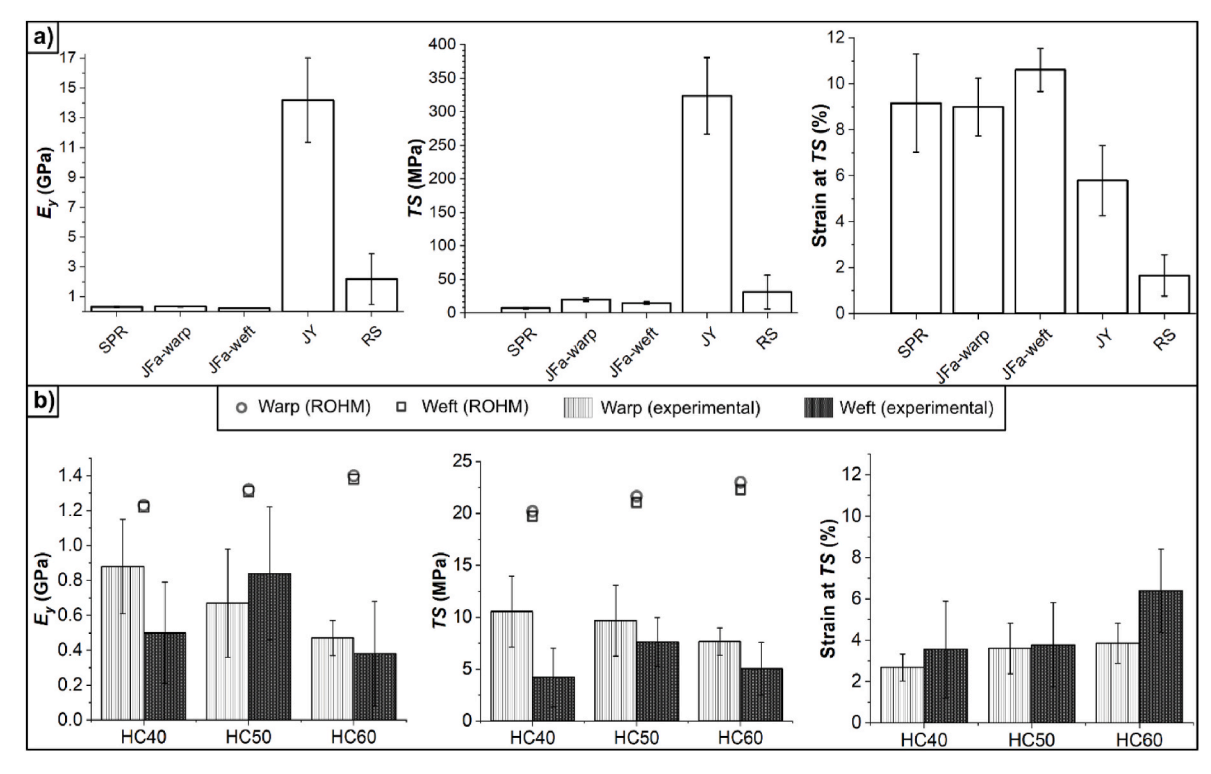


Fig. 9. Experimental tensile properties of a) constituents (SPR, JFa, JY, and RS), and their hybrid composites, as well as b) experimental and ROHM results of their hybrid composites (HC) at three different fiber loadings (40, 50, and 60%). Number of specimens (N) = 17 for SPR; N = 12 for each direction of JFa; N = 7 for JY; N = 53 for RS, N = 30–42 specimens for each single HC sample test.

idealized assumptions apply to the random oriented needle-punched natural fibers present in the tested composite systems. Comparing theory against experiment can help understand possible deficiencies in composite fabrication process and the defects introduced when fiber content is increased. A distinct possibility was that the resin was

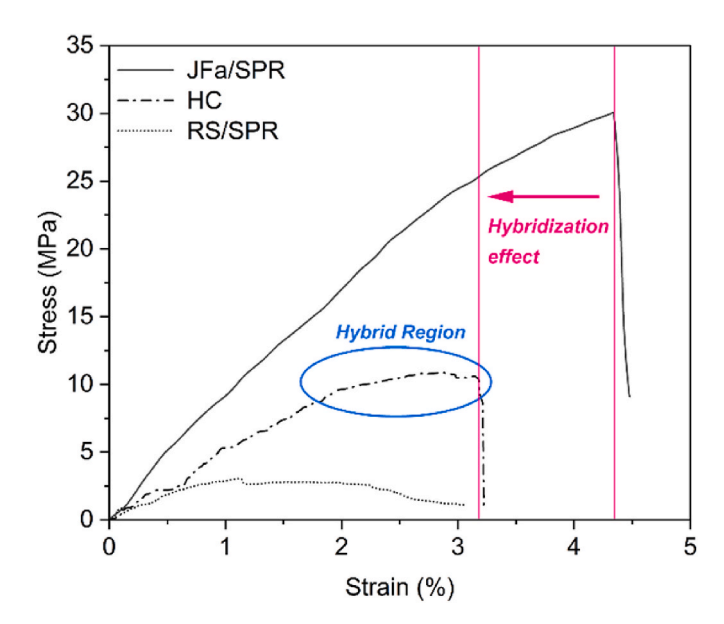
insufficient in wetting higher volumes of fibers which creates poor fiber/resin bonding and induces structural defects such as voids, air bubble, etc., in PMCs [65–68].

#### 3.3.3. Tensile properties of hybrid composites

Fig. 10 shows typical stress-strain plots of a hybrid JFa/RS/SPR composite (HC) and two non-hybrid composites: JFa/SPR and RS/SPR. Stress-strain plots of fabric reinforced PMC (JFa/SPR) start with a semilinear increase in load until maximum tensile stress or *TS*, followed by sharp (brittle) fall in the stress, such as that seen in Fig. 10 for JFa/SPR, confirming the dominance of JFa in Jfa/SPR composite. Hybrid composites, on the other hand, typically undergo a stress plateau known as the *hybrid region*, as circled in Fig. 10 [64]. In this region, premature consecutive crack propagation occurs primarily in the brittle fiber (RS) which transfers more load to the other intact fibers, JFa, in this case. This consequently creates higher stress levels, locally, for the stronger fibers causing them to fail at lower strains.

The strain to achieve TS decreased from 4.14% in JFa/SPI to 2.68% in HC, resulting in a 54.5% hybridization effect on strain [64]. Looking at the RS/SPR plot, given that RS fibers were random-sized and non-directional, the stress sharing between RS fibers did not fail consecutively in a rapid fashion beyond TS. Instead, an arch-shaped stress-strain plot corresponding to stress transfer between fibers was observed. This allows breaking of the brittle fibers located within the segment under test. Thus, the exhausted viscoelastic resin becomes the main load bearer and fails at almost two-thirds below its non-reinforced strain. Fig. 9b summarizes the tensile properties of the three hybrid composites tested along the warp and weft directions. In the warp direction,  $E_{\rm v}$  decreased by 31.3% and 42.6% as the fiber content increased from HC40 to HC50 and HC50 to HC60, respectively; with HC40 showing the highest  $E_v$  of 0.88  $\pm$  0.27 GPa. While in the weft direction, HC50 exhibited an  $E_v$  equal to 0.84  $\pm$  0.38 GPa, which is 69.8% higher than HC40 and 120.4% higher than HC60. This  $E_v$  value of HC50 in the weft direction is statistically indistinguishable from that of the stiffest warp composite, i.e., HC40, indicating the high disorientation caused by needle-punching. Moreover, it is expected that higher fiber loads would increase stiffness and water plasticization resistance, since water plasticization primarily occurs in the resin. However, the observed trends imply a weak fiber/resin interface. Also, the dominance of SPR mechanical properties-particularly compliance-is quite obvious in all HCs from data in Fig. 9a.

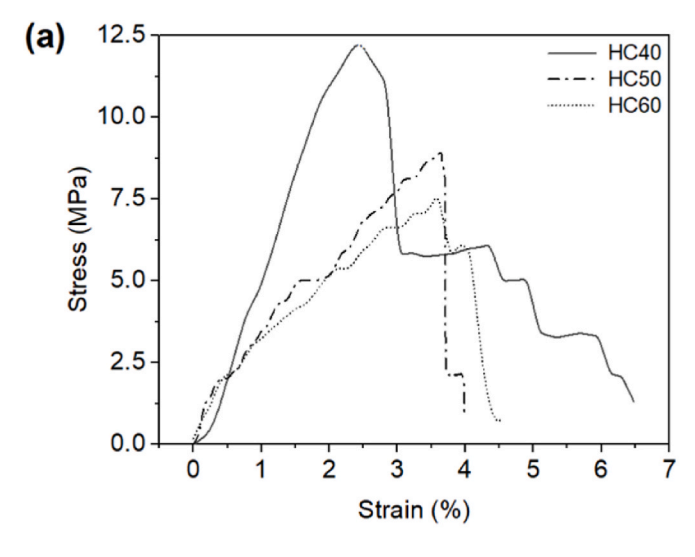
As for TS, all warp HCs surpassed the strengths of their corresponding weft counterparts. Similar to  $E_y$  trends, HCs weakened with increased fiber content; a direct result of the weak lower density RS



**Fig. 10.** Typical stress-strain plots of three conditioned composites: nonhybrid JFa/SPR, hybrid composite (HC), and nonhybrid RS/SPR. All composites contain 40 wt% fiber.

fibers occupying the majority of fiber reinforcement volume, hence inducing structural defects within the composites. Despite that result, SPR's strength was enhanced to up to 46.5% by the hybrid RS/JFa reinforcement. The strains at TS locations were indistinguishable between five of the six tested samples. The exception being HC60 in the weft with a value of  $6.4 \pm 4.1\%$ ; while the average of the means of the remaining composites was  $3.5 \pm 0.5\%$ .

Fig. 11 presents typical stress-strain plots for the hybrid composites obtained from conservative (65% RH) ASTM tensile tests, performed in the warp and weft directions. A brittle-like behavior can be inferred from all plots. It is also obvious that TS overlaps the yield point in most cases (except HC60 in the weft), and that fracture propagation happens rapidly afterwards. Hybridization as well as random geometries and orientation of RS divert the applied uniaxial stress along the fibers in shear, leading to extended stress-bearing at lower loads. Furthermore, all plots in Fig. 11 show a stepwise stress incline right until TS, as well as a random-fashioned rapid decline thereafter. This behavior is similar to the typical tensile response of fabrics, as mentioned earlier, with loss of crimp (slack), untwisting, and uncrimping noticed at the beginning of the stress-strain curve. In Fig. 11a, the relatively high resin volume of composites HC40 overcomes the weak fiber/resin interface. The mechanical responses of HC50 and HC60 exhibit notable step around the ~2.40 MPa and 4.00 MPa, which can be attributed to RS and JF IFSS debonding values, respectively. As for the weft direction, Fig. 11b, both



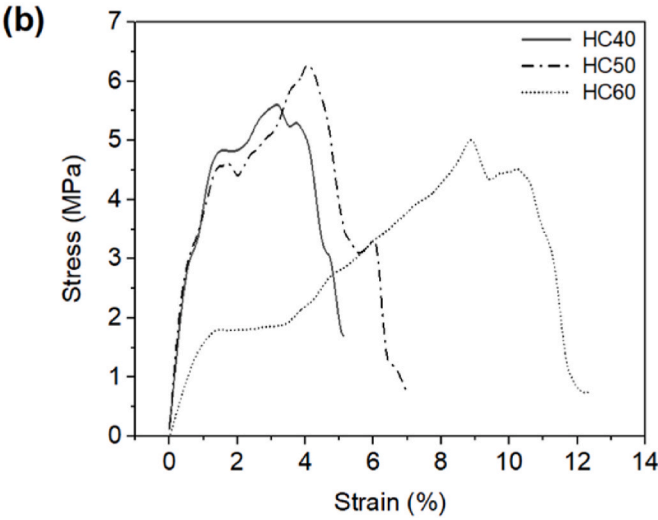


Fig. 11. Typical stress-strain plots of HC in a) warp direction, and b) weft direction.

HC40 and HC50 exhibit similar behavior. This may indicate that the needle-punching have disrupted the structure more prominently in the weft direction, which is typically mediated by the slack in weaving the weft yarns through the tightly held warp yarns during the fabric manufacturing. Looking closely at HC60 in the weft direction seen in Fig. 11b, an elastic behavior of the composite is observed until approximately 2 MPa. After which, the mechanical response is dominated by the strongest element in the composite, JFa, in the present case.

#### 3.4. Flexural properties

Fig. 12a and b depict typical stress-strain plots obtained from HC three-point flexural tests. Before conditioning, the step-like failure behavior observed (Fig. 12a), seems to reduce with increased fiber content. It may be caused by the decrease in specimen thicknesses at higher fiber content (which were  $\sim 3.58$  mm,  $\sim 3.23$  mm,  $\sim 3.10$  mm for HC40, HC50, HC60 specimens, respectively). However, and contrary to the theory, flexural strengths (*FS*) of the composites were affected by increasing fiber content, particularly for 60% fiber content. For example, *FS* for HC50 (14.03 MPa) was 14.5% less than HC40 (15.43 MPa), and remarkably, *FS* of HC60 (5.34 MPa) was 54.4% less than HC50, as seen in Fig. 12c. These characteristics confirm that fiber content exceeded the resin's optimal fiber wetting capacity, possibly even at the HC40 systems. One reason for this may be the higher viscosity of the resin that may not flow around fibers easily.

The effect of hybrid reinforcement layers, despite the RS/JFa interlacement, can be distinguished from the plots. A sequence of sharp failure modes followed by smoother ones (as Fig. 12a shows) corresponds to fracture propagation through the triple RS/JFa layers. The lack of sharp drops/peaks in stress after conditioning, as seen in Fig. 12b, indicates that water-induced resin plasticization has held the composite together, enhanced its flexibility, and distributed the load more evenly. HC60 exhibits the smallest flexural property loss due to water absorption with no significant drop in both  $E_f$  and FS, since HC60 lacks the

major water absorber, i.e., SPR. Water-induced resin plasticization shifted *FS* to higher strains, specifically to 90%, 53%, and 6% for HC40, HC50, and HC60, respectively, as can be expected.

#### 3.5. SEM fracture analysis

During tensile tests, all HCs fractured in a brittle fashion as seen in Fig. 13 SEM images of the fracture surfaces. HC40 specimen in Fig. 13a shows broken fibers within a close distance to the resin fracture surface. This implies either sufficient fiber/resin interfacial bonding or the availability of sufficient amounts of resins surrounding the fibers and holding them, or both. Given the relatively weak IFSS value and the fact that the SEM micrographs were taken after fracture; the more probable explanation is that enough resin was present around most fibers. The magnified jute fiber in Fig. 13a is seen fully coated with SPR, indicating successful resin impregnation into the depths of the composite. With increasing fiber content, longer lengths of fibers were pulled out from the resin's fracture surface. Some HC50 fracture regions with higher resin content show congruent constituents' fracture surfaces, such as the points marked with "x" in Fig. 13b. While other regions show fibers being pulled out a few hundred micrometers away from SPR, as can be seen between the "x" marks and the tip of the broken fibers in Fig. 13b. In this case, consecutive fracture modes could have occurred. First, fiber/resin debonding possibly took place and drastically increased the stress on SPR leading it to break. Then, fibers (or fiber bundles with enough resin in between them) were pulled out as they shared the load to failure. A similar but more exaggerated behavior was observed in the HC60 specimens as seen in Fig. 13c. Visually, fibers are highly disoriented with no obvious fracture surfaces. In this case, SPR volume was clearly surpassed by the high fiber volume present, causing fibers to debond, delaminate, and disorganize. In this case the resin clearly seems to be insufficient to cover all fibers.

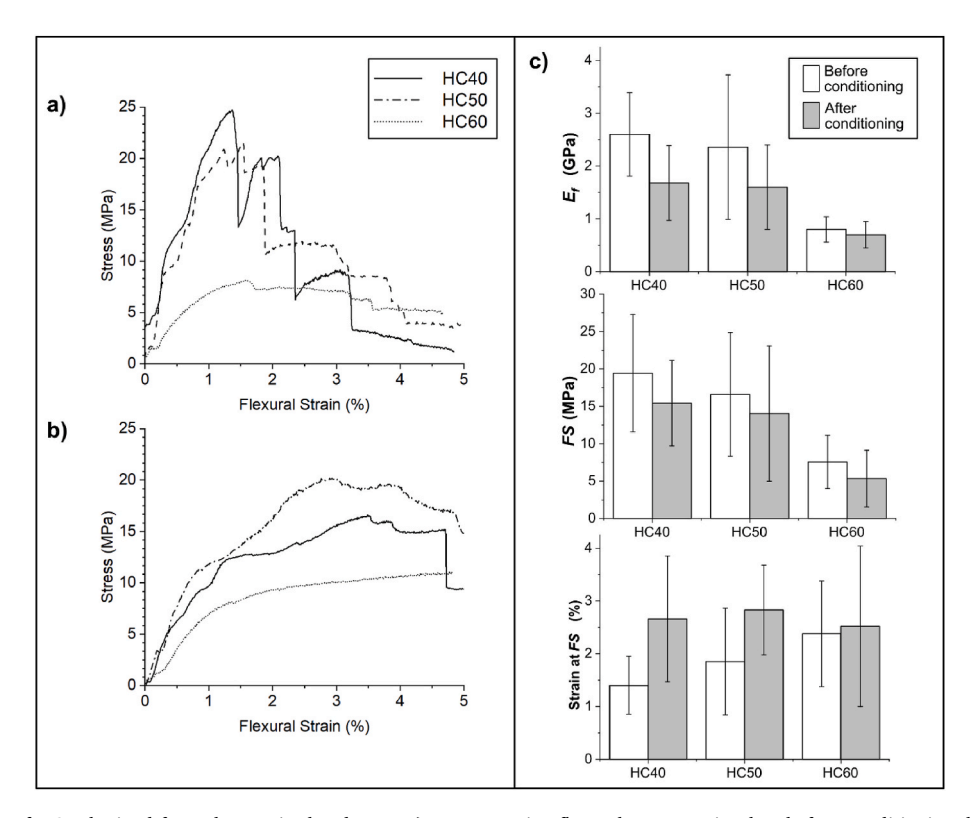


Fig. 12. Flexural results of HCs obtained from three-point-bend tests: a) representative flexural stress-strain plots before conditioning, b) representative flexural stress-strain plots after conditioning, c) flexural properties of interest comparing before and after conditioning. N = 18-19 specimens for each sample test.

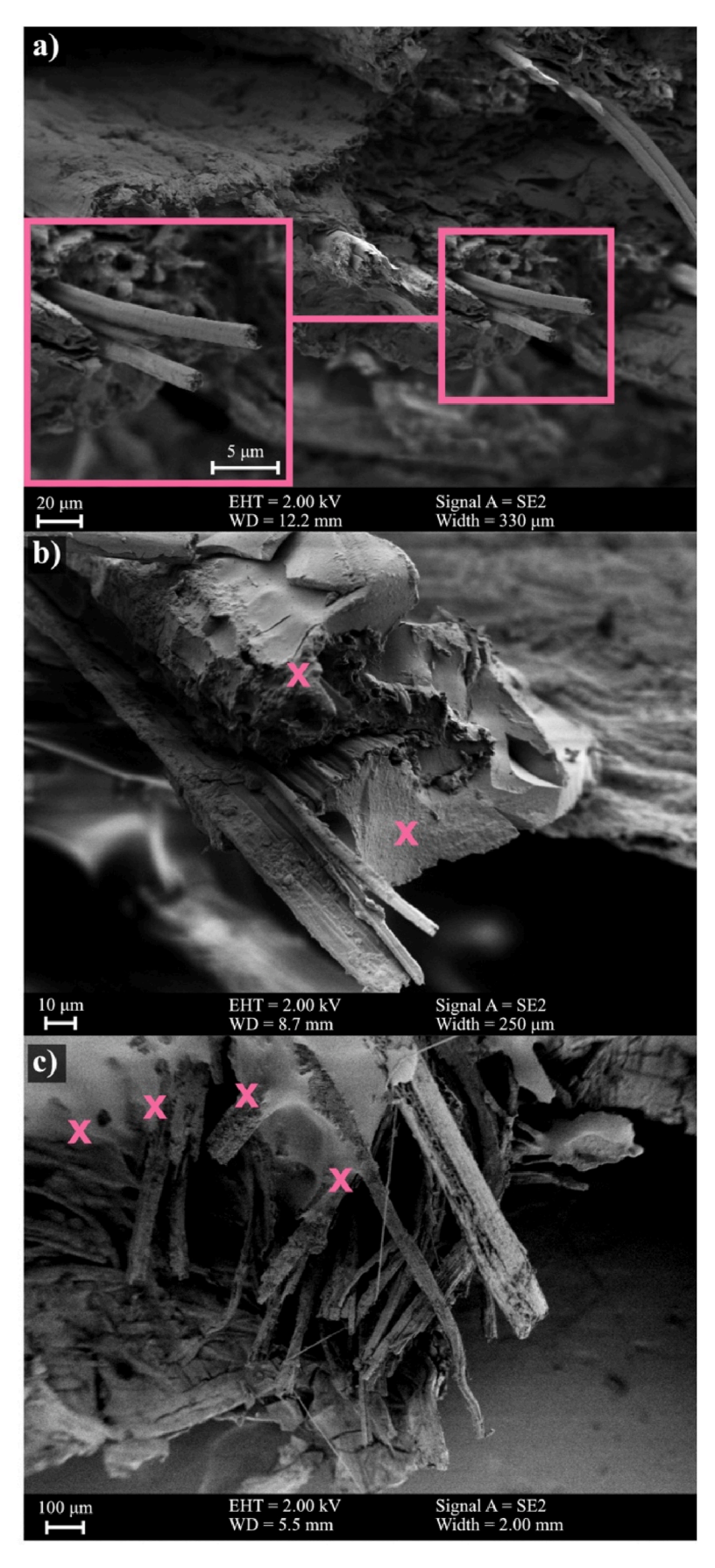


Fig. 13. SEM images showing fracture surfaces of hybrid composites after tensile failure for a) HC40, b) HC50, and c) HC60. Note: (×) marks denote SPR resin sites.

#### 4. Conclusions

Prototype hybrid green composites (with surface area equal to 0.254 m  $\times$  0.254 m) were fabricated using rice straw and jute fabric and a soy protein isolate-based resin. RS were needle-punched into woven JFa to produce a hybrid nonwoven interlaced RS/JFa mat. Crosslinked and plasticized SPI-based resin was impregnated into three layers of RS/JFa hybrid reinforcement mats, at three fiber weight fractions (40, 50 and 60%), termed as HC40, HC50, and HC60.

Characterization of interfacial shear strength, tensile properties, flexural properties, fracture, and water absorption of composites and their constituents lead to the following conclusions. All hybrid composites, except HC40, indicated insufficient resin volumes to fully surround the fibers. This was evident from the relatively longer protrusions of fibers at composite fracture surfaces seen in SEM fracture surface images of HC50 and HC60. Insufficient fiber-wetting increase fiber-fiber interactions over fiber-resin ones. Furthermore, structural distortions (as the weft direction of JFa was more prone to, during needle-punching) seemed to reduce the tensile properties of the HCs. All composites exhibited higher ultimate tensile strength (TS) in the warp direction compared to those in the weft direction. This is due to higher strength of JFa in warp direction and an indication of needle-punching process distorting the woven fabrics-more prominently in the weft yarns. The RS/JFa reinforcement, nonetheless, worked well in reinforcing the green SPR resin by enhancing its  $E_v$  and TS by up to 175% and 47%, respectively. Effect of water plasticization of SPR on flexural properties of the HCs was seen in the form of smoothening of stress-strain curves after conditioning. SPR plasticizing was also evident in increased strain at FS after conditioning, which were 90%, 53%, and 6% for HC40, HC50, and HC60, respectively. This plasticization effect directly correlated to the amount of resin in the hybrid composite. With tests performed at higher span ratios and strain rates than recommended by ASTM, none of the conditioned composites exhibited complete rupture below 5% strain. The stress-strain plots indicate more even load distributions and less dramatic stress losses post conditioning. The anisotropy and internal defects of the three-layered composites could possibly be compensated for by increasing the number of layers; as well as higher resin volume. Green hybrid composites (consisting mostly of weak lignocellulosic fibers needle-punched into stronger dense fibers) have demonstrated to be an effective approach to utilize plant fiber waste. The green hybrid composites produced in this study have properties to work as green alternatives in paneling, housing, or packaging applications by replacing wood and wood-based products such as plywood, medium density fiber boards, and particle boards that are currently used.

# Credit author statement

Abdullah Alkandary: Conceptualization, Visualization, Experimental Work, Original draft, Editing.

Anil Netravali: Conceptualization, Supervision, Review, Resources, Editing, Project administration.

# Declaration of competing interest

The authors declare that they have no known competing financial interests or personal relationships that could have appeared to influence the work reported in this paper.

# Data availability

No data was used for the research described in the article.

#### Acknowledgements

The authors acknowledge the partial financial support provided by Tata-Cornell Institute. Archer-Daniels-Midland Company (Chicago, IL)

for their generous donation of soy protein isolate. The use of the Cornell Center for Materials Research Shared Facilities, which are supported through the NSF MRSEC program (DMR-1719875), is acknowledged. Also, the Kuwait Institute for Scientific Research for generously funding Abdullah Alkandary's graduate study at Cornell University.

#### References

- [1] Netravali AN, Chabba S. Composites get greener. Mater Today 2003;6:22–9. https://doi.org/10.1016/S1369-7021(03)00427-9.
- [2] Luo S, Netravali AN. Mechanical and thermal properties of environment-friendly "green" composites made from pineapple leaf fibers and poly(hydroxybutyrate-covalerate) resin. Polym Compos 1999;20:367–78. https://doi.org/10.1002/ pc.10363
- [3] Luo S, Netravali AN. Interfacial and mechanical properties of environment-friendly "green" composites made from pineapple fibers and poly(hydroxybutyrate-co-valerate) resin. J Mater Sci 1999;34:3709–19. https://doi.org/10.1023/A: 1004659507231.
- [4] Chamas A, Moon H, Zheng J, Qiu Y, Tabassum T, Jang JH, Abu-Omar M, Scott SL, Suh S. Degradation rates of plastics in the environment. ACS Sustainable Chem Eng 2020;8:3494–511. https://doi.org/10.1021/acssuschemeng.9b06635.
- [5] Geyer R, Jambeck JR, Law KL. Production, use, and fate of all plastics ever made. Sci Adv 2017;3:25–9. https://doi.org/10.1126/sciadv.1700782.
- [6] Zheng J, Suh S. Strategies to reduce the global carbon footprint of plastics. Nat Clim Change 2019;9:374–8. https://doi.org/10.1038/s41558-019-0459-z.
- [7] Bakis CE, Bank LC, Brown VL, Cosenza E, Davalos JF, Lesko JJ, Machida A, Rizkalla SH, Triantafillou TC. Fiber-reinforced polymer composites for construction - state-of-the-art review. Perspect. Civ. Eng. Commem. 150th Anniv. Am. Soc. Civ. Eng. 2003;6:369–83. https://doi.org/10.1061/(asce)1090-0268. 2002)6:2(73.
- [8] USDA Economic Research Service: Soybeans & Oil Crops, (n.d.). https://www.ers. usda.gov/topics/crops/soybeans-oil-crops/.
- [9] Truax TR. The gluing of wood. Washington, D.C.: U.S. Dept. of Agriculture; 1929. https://doi.org/10.5962/bhl.title.108492.
- [10] Liu C, Zhang Y, Li X, Luo J, Gao Q, Li J. Green" bio-thermoset resins derived from soy protein isolate and condensed tannins. Ind Crop Prod 2017;108:363–70. https://doi.org/10.1016/j.indcrop.2017.06.057.
- [11] Yang Z, Peng H, Wang W, Liu T. Crystallization behavior of poly(e-caprolactone)/ layered double hydroxide nanocomposites. J Appl Polym Sci 2010;116:2658–67. https://doi.org/10.1002/app.
- [12] Lodha P, Netravali AN. Characterization of interfacial and mechanical properties of "green" composites with soy protein isolate and ramie fiber. J Mater Sci 2002;37: 3657–65. https://doi.org/10.1023/A:1016557124372.
- [13] Petruccelli S, Añón MC. Soy protein isolate components and their interactions. J Agric Food Chem 1995;43:1762–7. https://doi.org/10.1021/jf00055a004.
- [14] Silva NHCS, Vilela C, Marrucho IM, Freire CSR, Pascoal Neto C, Silvestre AJD. Protein-based materials: from sources to innovative sustainable materials for biomedical applications. J Mater Chem B 2014;2:3715–40. https://doi.org/ 10.1039/c4tb00168k.
- [15] Song F, Tang DL, Wang XL, Wang YZ. Biodegradable soy protein isolate-based materials: a review. Biomacromolecules 2011;12:3369–80. https://doi.org/ 10.1021/bm200904x.
- [16] Chhavi Deepmala KM, Singh VK, Jain N. Soy protein based green composite: a review. 05 Res Rev J Mater Sci 2017:66–77. https://doi.org/10.4172/2321-6212.1000171.
- [17] Patil NV, Netravali AN. Enhancing strength of wool fiber using a soy flour sugar-based "green" cross-linker. ACS Omega 2019;4:5392–401. https://doi.org/10.1021/acsomega.9b00055.
- [18] Lodha P, Netravali AN. Characterization of phytagel® modified soy protein isolate resin and unidirectional flax yarn reinforced "Green" composites. Polym Compos 2005;26:647–59. https://doi.org/10.1002/pc.20128.
- [19] Lodha P, Netravali AN. Thermal and mechanical properties of environment-friendly "green" plastics from stearic acid modified-soy protein isolate. Ind Crop Prod 2005;21:49–64. https://doi.org/10.1016/j.indcrop.2003.12.006.
- [20] Lodha P, Netravali AN. Characterization of stearic acid modified soy protein isolate resin and ramie fiber reinforced "green" composites. Compos Sci Technol 2005;65: 1211–25. https://doi.org/10.1016/j.compscitech.2004.12.036.
- [21] Ghosh Dastidar T, Netravali A. Cross-linked waxy maize starch-based "green" composites. ACS Sustainable Chem Eng 2013;1:1537–44. https://doi.org/10.1021/ sc400113a.
- [22] Dastidar TG, Netravali AN, Ghosh Dastidar T, Netravali AN. A soy flour based thermoset resin without the use of any external crosslinker. Green Chem 2013;15: 3243–51. https://doi.org/10.1039/c3gc40887f.
- [23] V Patil N, Rahman MM, Netravali AN. Green" composites using bioresins from agro-wastes and modified sisal fibers. Polym Compos 2019;40:99–108. https://doi. org/10.1002/pc.24607.
- [24] Patil NV, Netravali AN. Microfibrillated cellulose-reinforced nonedible starch-based thermoset biocomposites. J Appl Polym Sci 2016;133:1–9. https://doi.org/10.1002/app.43803.
- [25] Huang X, Netravali A. Biodegradable green composites made using bamboo micro/ nano-fibrils and chemically modified soy protein resin. Compos Sci Technol 2009; 69:1009–15. https://doi.org/10.1016/j.compscitech.2009.01.014.
- 69:1009–15. https://doi.org/10.1016/j.compscitech.2009.01.014.
  [26] Kim JR, Netravali AN. Self-healing green composites based on soy protein and microfibrillated cellulose. Compos Sci Technol 2017;143:22–30. https://doi.org/10.1016/j.compscitech.2017.02.030.

- [27] Kim JR, Netravali AN. Comparison of thermoset soy protein resin toughening by natural rubber and epoxidized natural rubber. J Appl Polym Sci 2017;134:1–13. https://doi.org/10.1002/app.44665.
- [28] Kim JR, Netravali AN. Self-Healing properties of protein resin with soy protein isolate-loaded poly(d,l-lactide-co-glycolide) microcapsules. Adv Funct Mater 2016; 26:4786–96. https://doi.org/10.1002/adfm.201600465.
- [29] Jariwala H, Jain P. A review on mechanical behavior of natural fiber reinforced polymer composites and its applications. J Reinforc Plast Compos 2019;38:441–53. https://doi.org/10.1177/0731684419828524.
- [30] Summerscales J, Dissanayake NPJ, Virk AS, Hall W. A review of bast fibres and their composites. Part 1 - fibres as reinforcements. Compos Part A Appl Sci Manuf 2010;41:1329–35. https://doi.org/10.1016/j.compositesa.2010.06.001.
- [31] Sahu P, Gupta MK. A review on the properties of natural fibres and its biocomposites: effect of alkali treatment. Proc Inst Mech Eng Part L J Mater Des Appl 2020;234:198–217. https://doi.org/10.1177/1464420719875163.
- [32] Burrola-Núñez H, Herrera-Franco PJ, Rodríguez-Félix DE, Soto-Valdez H, Madera-Santana TJ. Surface modification and performance of jute fibers as reinforcement on polymer matrix: an overview. J Nat Fibers 2019;16:944–60. https://doi.org/10.1080/15440478.2018.1441093.
- [33] Khandanlou R, Ahmad MB, Shameli K, Hussein MZ, Zainuddin N, Kalantari K. Effect of unmodified rice straw on the properties of rice straw/polycaprolactone composites. Res Chem Intermed 2015;41:6371–84. https://doi.org/10.1007/ s11164-014-1746-v.
- [34] Bassyouni M, Taha I, Abdel-Hamid SMS, Steuernagel L. Physico-mechanical properties of chemically treated polypropylene rice straw bio-composites. J Reinforc Plast Compos 2012;31:303–12. https://doi.org/10.1177/ 0731684411436024.
- [35] Ming-Zhu P, Chang-Tong M, Xu-Bing Z, Yun-Lei P. Effects of rice straw fiber morphology and content on the mechanical and thermal properties of rice straw fiber-high density polyethylene composites. J Appl Polym Sci 2011;121:2900–7. https://doi.org/10.1002/app.33913.
- [36] Bassyouni M, Waheed Ul Hasan S. The use of rice straw and husk fibers as reinforcements in composites. In: Biofiber reinf. Compos. Mater. Elsevier; 2015. p. 385–422. https://doi.org/10.1533/9781782421276.4.385.
- [37] Hasan KMF, Horváth PG, Bak M, Le DHA, Mucsi ZM, Alpár T. Rice straw and energy reed fibers reinforced phenol formaldehyde resin polymeric biocomposites. Cellulose 2021;28:7859–75. https://doi.org/10.1007/s10570-021-04029-9.
- [38] Van Soest PJ. Rice straw, the role of silica and treatments to improve quality. Anim Feed Sci Technol 2006;130:137–71. https://doi.org/10.1016/j. anifeedsci.2006.01.023.
- [39] Domínguez-Escribá L, Porcar M. Rice straw management: the big waste. Biofuels, Bioprod Biorefining 2010;4:154–9. https://doi.org/10.1002/bbb.196.
- [40] Ren J, Yu P, Xu X. Straw utilization in China-status and recommendations. Sustain Times 2019;11:1–17. https://doi.org/10.3390/su11061762.
- [41] Hiziroglu S, Bauchongkol P, Fueangvivat V, Soontonbura W, Jarusombuti S. Selected properties of medium density fiberboard (MDF) panels made from bamboo and rice straw. For Prod J 2007;57:46–50.
- [42] Ratna Prasad AV, Murali Mohan Rao K, Mohan Rao K, Gupta A. Tensile and impact behaviour of rice straw-polyester composites. Indian J Fibre Text Res 2007;32: 399–403.
- [43] Liu Z, Xu A, Long B. Energy from combustion of rice straw: status and challenges to China. 03 Energy Power Eng 2011:325–31. https://doi.org/10.4236/ epe.2011.33040.
- [44] Van Nguyen H, Nguyen CD, Van Tran T, Hau HD, Nguyen NT, Gummert M. Energy efficiency, greenhouse gas emissions, and cost of rice straw collection in the mekong river delta of vietnam. Field Crop Res 2016;198:16–22. https://doi.org/ 10.1016/j.fcr.2016.08.024.
- [45] Said N, Abdel Daiem MM, García-Maraver A, Zamorano M. Influence of densification parameters on quality properties of rice straw pellets. Fuel Process Technol 2015;138:56–64. https://doi.org/10.1016/j.fuproc.2015.05.011.
- [46] Chen X, Chen L, Zhang C, Song L, Zhang D. Three-dimensional needle-punching for composites - a review. Compos Part A Appl Sci Manuf 2016;85:12–30. https://doi. org/10.1016/j.compositesa.2016.03.004.
- [47] Yamamoto Y, Zahora D, Netravali AN. Determination of the interfacial properties between modified soy protein resin and kenaf fiber. Compos Interfac 2007;14: 699–713. https://doi.org/10.1163/156855407782106456.

- [48] Kim JT, Netravali AN. Effect of protein content in soy protein resins on their interfacial shear strength with ramie fibers. J Adhes Sci Technol 2010;24:203–15. https://doi.org/10.1163/016942409X12538812532159.
- [49] Nam S, Netravali AN. Characterization of ramie fiber/soy protein concentrate (SPC) resin interface. J Adhes Sci Technol 2004;18:1063–76. https://doi.org/ 10.1163/1568561041257504.
- [50] Souzandeh H, Netravali AN. Study and characterization of sisal fiber/zein resin interface. Rev Adhes Adhes 2020;8. https://doi.org/10.7569/RAA.2018.097307. S1\_S19
- [51] Huang X, Netravali A. Characterization of flax fiber reinforced soy protein resin based green composites modified with nano-clay particles. Compos Sci Technol 2007;67:2005–14. https://doi.org/10.1016/j.compscitech.2007.01.007.
- [52] Moniruzzaman M, Du F, Romero N, Winey KI. Increased flexural modulus and strength in SWNT/epoxy composites by a new fabrication method. Polymer (Guildf) 2006;47:293–8. https://doi.org/10.1016/j.polymer.2005.11.011.
- [53] Ary Subagia IDG, Kim Y, Tijing LD, Kim CS, Shon HK. Effect of stacking sequence on the flexural properties of hybrid composites reinforced with carbon and basalt fibers. Compos B Eng 2014;58:251–8. https://doi.org/10.1016/j. compositesb.2013.10.027.
- [54] Mirbagheri J, Tajvidi M, Hermanson JC, Ghasemi I. Tensile properties of wood flour/kenaf fiber polypropylene hybrid composites. J Appl Polym Sci 2007;105: 3054–9. https://doi.org/10.1002/app.26363.
- [55] Fu SY, Xu G, Mai YW. On the elastic modulus of hybrid particle/short-fiber/ polymer composites. Compos B Eng 2002;33:291–9. https://doi.org/10.1016/ S1359-8368(02)00013-6.
- [56] Venkateshwaran N, Elayaperumal A, Sathiya GK. Prediction of tensile properties of hybrid-natural fiber composites. Compos B Eng 2012;43:793–6. https://doi.org/ 10.1016/j.compositesb.2011.08.023.
- [57] Miller B, Muri P, Rebenfeld L. A microbond method for determination of the shear strength of a fiber/resin interface. Compos Sci Technol 1987;28:17–32. https://doi. org/10.1016/0266-3538(87)90059-5.
- [58] Kalita D, Netravali AN. Interfaces in green composites: a critical review. Rev Adhes Adhes 2015;3:386–443. https://doi.org/10.7569/RAA.2015.097311.
- [59] Netravali AN, Henstenburg RB, Phoenix SL, Schwartz P. Interfacial shear strength studies using the single-filament-composite test. I: experiments on graphite fibers in epoxy. Polym Compos 1989;10:226–41. https://doi.org/10.1002/ pc.750100405
- [60] Pan N, Brookstein D. Physical properties of twisted structures. II. Industrial yarns, cords, and ropes. J Appl Polym Sci 2002;83:610–30. https://doi.org/10.1002/app.2261.
- [61] Rao Y, Farris RJ. Modeling and experimental study of the influence of twist on the mechanical properties of high-performance fiber yarns. J Appl Polym Sci 2000;77: 1938–49. https://doi.org/10.1002/1097-4628(20000829)77:9<1938::AID-APP9>3.0.CO:2. D.
- [62] Jeon BS. Evaluation of the structural properties of plain fabrics woven from various fibers using Peirce's model. Fibers Polym 2012;13:130–4. https://doi.org/ 10.1007/s12221-012-0130-z.
- [63] Zini E, Scandola M. Green composites: an overview. Polym Compos 2011;32: 1905–15. https://doi.org/10.1002/pc.21224.
- [64] Kretsis G. A review of the tensile, compressive, flexural and shear properties of hybrid fibre-reinforced plastics. Composites 1987;18:13–23. https://doi.org/ 10.1016/0010-4361(87)90003-6.
- [65] Satyanarayana KG, Arizaga GGC, Wypych F. Biodegradable composites based on lignocellulosic fibers-An overview. Prog Polym Sci 2009;34:982–1021. https://doi. org/10.1016/j.progpolymsci.2008.12.002.
- [66] Torres-Tello EV, Robledo-Ortíz JR, González-García Y, Pérez-Fonseca AA, Jasso-Gastinel CF, Mendizábal E. Effect of agave fiber content in the thermal and mechanical properties of green composites based on polyhydroxybutyrate or poly (hydroxybutyrate-co-hydroxyvalerate). Ind Crop Prod 2017;99:117–25. https://doi.org/10.1016/j.indcrop.2017.01.035.
- [67] Sanyang ML, Sapuan SM, Jawaid M, Ishak MR, Sahari J. Recent developments in sugar palm (Arenga pinnata) based biocomposites and their potential industrial applications: a review. Renew Sustain Energy Rev 2016;54:533–49. https://doi. org/10.1016/j.rser.2015.10.037.
- [68] Netravali A. Advanced green composites. John Wiley & Sons, Inc.; 2007.